Available online at www.sciencedirect.com
ScienceDirect
Journal of Catalysis 255 (2008) 190–196
JOURNAL OF CATALYSIS
www.elsevier.com/locate/jcat

Surface functionalization of SBA-15-ordered mesoporous silicas: Oxidation of benzene to phenol by nitrous oxide

Ying Li [a], Zhaochi Feng [b], R.A. van Santen [a], E.J.M. Hensen [a,*], Can Li [b,*]

[a] *Schuit Institute of Catalysis, Eindhoven University of Technology, P.O. Box 513, 5600 MB Eindhoven, The Netherlands*
[b] *State Key Laboratory of Catalysis, Dalian Institute of Chemical Physics, Chinese Academy of Sciences, Dalian 116023, China*

Received 27 November 2007; revised 3 February 2008; accepted 4 February 2008

Available online 7 March 2008

Abstract

We report the preparation and catalytic properties of highly ordered mesoporous Fe–Ga–SBA-15 materials via direct hydrothermal synthesis. Gallium and iron ions were introduced directly into the synthesis gel typical for the preparation of SBA-15. The resulting materials had hexagonally ordered mesopores of about 6 nm and surface areas >1000 m^2/g. In Fe–SBA-15, the iron species were mainly tetrahedrally coordinated in the amorphous silica walls. In the presence of Ga (Fe–Ga–SBA-15), Fe species were located at the silica surface as isolated species, as determined by Raman and diffuse-reflectance UV–Vis spectroscopy measurements. The Fe species in Fe–Ga–SBA-15 displayed similar properties as the FeZSM-5 zeolites toward nitrous oxide decomposition and were active in the oxidation of benzene to phenol by nitrous oxide. Ga–SBA-15 and Fe–SBA-15, on the other hand, showed no catalytic activity. Compared with Fe–Al–SBA-15, Fe–Ga–SBA-15 displayed greater selectivity to the desired phenol product.

Keywords: Selective oxidation; Benzene; Nitrous oxide; Fe–Ga–SBA-15; Ordered mesoporous silica; Active sites; Resonance Raman spectroscopy

1. Introduction

Ordered mesoporous silicas, such as MCM-41 and SBA-15, have received considerable attention owing to their high surface area and pore volume, as well as their well-ordered arrangement of uniformly sized mesopores. These textural properties make them useful as catalyst supports [1–4]. SBA-15 material is synthesized in acidic medium with poly(alkylene oxide) tri-block copolymers under relatively mild synthesis conditions [4]. Numerous studies have dealt with the introduction of metal ions, such as Al, Co, Ti, V, Cr, B, Fe, and Ga, in amorphous silica walls [5–8] to modify the chemical properties. Substitution or surface functionalization is important to functionalize the surface with catalytically active acidic or redox sites. SBA-15 is more promising than MCM-41 for catalytic applications, because the thicker silica walls give the material greater hydrothermal stability [4].

There is a desire to prepare uniformly distributed and preferably isolated sites on silica surfaces, which is crucial for high activity and selectivity. The controlled synthesis of well-defined iron species in amorphous silica supports remains a challenge. The amorphous nature of the silica walls most often results in poorer catalytic performance than encountered for microporous crystalline zeolites. A well-known example of the specific reactivity of cation-modified zeolites is iron-containing ZSM-5. FeZSM-5 zeolites are known for their promising catalytic activity in the selective oxidation of benzene to phenol [9–13]. Because this reaction has some potential to replace the cumene process in phenol production, FeZSM-5 zeolites have been studied in great detail. Although no consensus has been reached regarding the nature of the iron centers, it is clear that the extra-framework Fe species form the active sites. Aluminum is also reported to be important for good catalytic performance [12,13]. Recently, we reported that simultaneous introduction of Fe and Al in the synthesis gel to produce SBA-15 results in catalysts that exhibit catalytic activity in the oxidation of benzene to phenol with nitrous oxide [14,15]. The role of aluminum is most likely related to a cationic-exchange site in the silica

* Corresponding authors.
E-mail addresses: e.j.m.hensen@tue.nl (E.J.M. Hensen), canli@dicp.ac.cn (C. Li).

0021-9517/$ – see front matter
doi:10.1016/j.jcat.2008.02.001

surface where surface Fe species can be stabilized. Indeed, in the absence of aluminum, only very low amounts of iron are introduced in SBA-15, and most of these ions are part of the bulk of the silica.

In the present work, we investigated the effect of Ga ions on the location and catalytic activity of Fe species in SBA-15 materials. We used UV–Vis spectroscopy to study the degree of clustering of the iron species and resonance Raman spectroscopy to identify the isolated transition metal ions [16–19]. We evaluated catalytic performance by oxidation of benzene to phenol with nitrous oxide as the oxidant.

2. Experimental

2.1. Preparation

Fe–Ga–SBA-15 samples were prepared by a direct hydrothermal synthesis procedure. Gallium was added as gallium nitrate during prehydrolysis of tetramethylorthosilicate (TMOS), to which the iron precursor, iron(III) nitrate, was added. In a typical synthesis procedure for Fe–Ga–SBA-15 materials, 2 g of P123 surfactant (Aldrich) was dissolved in 70 mL of HCl solution at pH value of 1.5 (solution A). TMOS (Aldrich, 3.2 mL), an appropriate amount of iron nitrate (Fe/Si molar ratio = 0.01 and 0.03), and 0.5384 g of gallium nitrate (Ga/Si = 0.10) were mixed with 5 mL of deionized water to obtain solution B. Solution B was stirred at room temperature for 20 min to obtain a clear solution, which was then added dropwise to solution A. The mixture of solutions A and B was stirred vigorously for 20 h at 313 K and then transferred to a Teflon-lined autoclave and aged for 24 h at 373 K. The resulting solid was filtered, washed, and dried at 333 K for 15 h. Finally, the mesoporous Fe–Ga–SBA-15 materials were obtained by calcination in artificial air at 773 K for 10 h. Characterization was carried out on the calcined samples. The catalysts are designated by their Fe/Si molar ratio (x) as Fe–Ga–SBA-15(x). Fe–SBA-15 (Fe/Si = 0.03) and Ga–SBA-15 (Ga/Si = 0.10) were prepared in the same manner without the addition of gallium and iron nitrate, respectively.

2.2. Characterization

The Fe and Ga loadings were determined by ICP-OES after an aliquot of the sample was dissolved in a mixture of HF and HNO_3. XRD spectra were recorded on a Rigaku D/Max 3400 powder diffraction system using Cu$K\alpha$ radiation (40 kV and 36 mA) over the range $0.5 \leqslant 2\theta \leqslant 10$ degrees. Nitrogen sorption isotherms were determined at 77 K on a Micromeritics ASAP2020 system in static measurement mode. The samples were outgassed at 573 K for 10 h before the sorption experiments. The pore size distribution was calculated by analyzing the desorption branch of the isotherm by the BJH (Barrett–Joyner–Halenda) method.

Diffuse reflectance UV–Vis spectra in the range of 200–800 nm were obtained using a JASCO V-550 UV–Vis spectrophotometer equipped with a diffuse reflectance attachment against a BaSO4 reference. Raman spectra were collected at room temperature using a Jobin-Yvon T64000 triple-stage spectrograph with a spectral resolution of 2 cm^{-1}. The 325-nm laser line of a He–Cd laser was used as the exciting source, with an output power of 30 mW. The power of the laser at the sample was about 3.0 mW. The 266-nm laser line was obtained by frequency doubling of a Coherent Verdi 10 laser (532 nm, output power 1 W) with a Spectra-Physics WaveTrain external frequency doubler. The power of the 266-nm line at the sample was about 3.0 mW. The 244-nm laser from a Coherent Innova 300 Fred laser was used as the excitation source in the deep UV region; its power at the sample was <1.0 mW.

2.3. Catalytic activity

Reaction data were collected using a plug flow reactor operating at atmospheric pressure as described in detail elsewhere [13]. For the oxidation of benzene to phenol by nitrous oxide, typically 0.1 g of catalyst (sieve fraction 125–425 μm) was mixed with SiC. Benzene was fed to the reaction mixture through a liquid mass flow controller (Bronkhorst). The final feed mixture contained 1 vol% benzene and 4 vol% nitrous oxide in helium at a total flow rate of 100 mL min^{-1}. The gas hourly space velocity was 30,000 h^{-1}. All valves and most tubing of the reaction system was placed in an oven system and heated to 453 K, to avoid condensation of heavy product molecules. The gas-phase composition was determined by a combination of online gas chromatography (Hewlett-Packard GC-5890 equipped with an HP-5 column and a flame ionization detector) and mass spectrometry (Balzers TPG-215). The reaction products included phenol, water, carbon monoxide, and carbon dioxide. The nitrous oxide and benzene conversions, nitrous oxide selectivity (i.e., the fraction of oxygen atoms from nitrous oxide incorporated in phenol), benzene selectivity (i.e., the fraction of benzene converted to phenol), and the rate of phenol formation were calculated. The carbon and nitrogen mass balances closed at 98% after prolonged reaction times.

3. Results and discussion

3.1. Catalyst characterization

Table 1 lists the elemental composition of the gel and the products. Fig. 1 shows the powder XRD patterns for the various materials. The low-angle region exhibits the typical features of a well-ordered mesoporous materials arranged in a two-dimensional hexagonal structure [4]. No diffraction features due to iron oxide or gallium oxide aggregates were found in the high-angle region (patterns not shown).

The textural properties of the mesoporous materials were analyzed by nitrogen porosimetry. The isotherms presented in Fig. 2 can be classified as type IV with an H1 hysteresis loop; the relevant data are given in Table 1. The isotherms are typical of mesoporous materials with the $p6_3/mm$ arrangement of pores with large diameter and a relatively narrow pore size distribution. The well-defined step occurring at relative high pressures of 0.6–0.8, corresponding to capillary condensation of nitrogen, points to the uniformity of the pores [20]. The pore

Table 1
Physicochemical characterization of the various mesoporous materials and a typical steam-activated FeZSM-5 catalyst

Catalyst	Molar gel ratio Ga/Si	Final Ga (wt%)	Molar gel ratio Fe/Si	Final Fe (wt%)	a_0[a] (nm)	Surface area (m^2/g)	Pore volume (cc/g)	Pore diameter[b] (nm)	N_α (mmol/g)[c]
Ga–SBA-15	0.10	3.63	0	–	10.8	967	1.26	7.3	0
Fe–SBA-15	–	–	0.03	0.14	12.6	1172	1.31	6.4	0
Fe–Ga–SBA-15(0.01)	0.10	3.33	0.01	0.11	12.0	1011	1.33	6.1	n.d.[d]
Fe–Ga–SBA-15(0.03)	0.10	2.73	0.03	0.21	12.3	1091	1.34	6.3	0.88×10^{-3}
Fe–Al–SBA-15	0.10[d]	3.27[e]	0.005	0.21	12.5	780	1.28	8.2	0.90×10^{-3}
FeZSM-5[f]	–	0.88[e]	–	0.45	–	413[g]	0.15	–	1.21×10^{-2}

[a] a_0 calculated from the d_{100} reflection according to $a_0 = 2 \times d_{100}/\sqrt{3}$.
[b] Calculated from the desorption branch of the isotherm according to the BJH method.
[c] Number of α-sites as determined by nitrous oxide decomposition at 523 K.
[d] Not determined.
[e] Refers to Al instead of Ga.
[f] From Ref. [12].
[g] Calculated according to the Dubinin–Radhovich method.

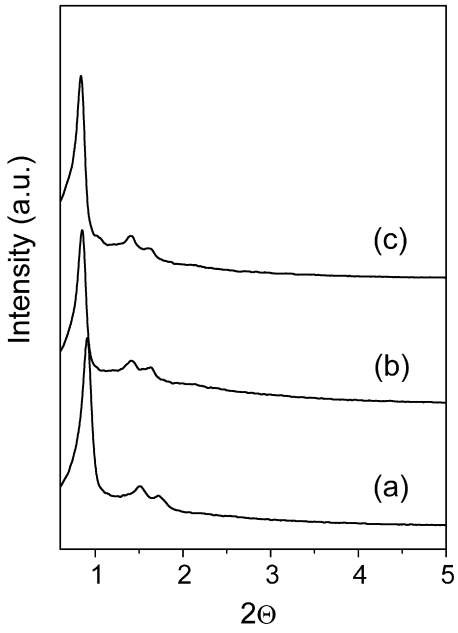

Fig. 1. Powder XRD patterns of calcined (a) Ga–SBA-15, (b) Fe–Ga–SBA-15(0.01) and (c) Fe–Ga–SBA-15(0.03).

diameters of the Fe–Ga–SBA-15 materials were around 6 nm, with surface areas >1000 m^2/g. From the a_0 value of about 12 nm, we calculate a wall thickness of about 6 nm. For Ga–SBA-15, the walls were somewhat thinner (~4 nm). The typical pore wall thickness of SBA-15 silica is ca. 4 nm [4]. This suggests that incorporation of Fe resulted in increased SBA-15 wall thickness. The thicker pore walls of Fe–Ga–SBA-15 should confer greater hydrothermal stability, which is beneficial in catalytic applications. The transmission electron micrographs of calcined Fe–Ga–SBA-15 given in Fig. 3 clearly show the well-ordered hexagonal arrays of the mesopores. The morphology of this material is typical of SBA-15 materials.

Fig. 4 shows the diffuse reflectance UV–Vis spectra of calcined Fe–Ga–SBA-15(0.01) and Fe–Ga–SBA-15(0.03). The spectra exhibit an intense absorption band at 270 nm that is assigned to isolated Fe^{3+} ions in an octahedral or pseudotetrahedral environment [21,22]. The intensity of this band increases with the Fe content. The absence of a tail at longer wavelengths in the 300–600 nm region indicates that the Fe-containing catalysts are free of aggregated iron oxide clusters. The spectrum of Ga–SBA-15 (not shown) exhibited no absorption bands.

Fig. 5 (above) compares the UV–Vis spectra of Fe–SBA-15 (0.14 wt% Fe) and Fe–Ga–SBA-15 (0.21 wt% Fe). The UV–Vis spectrum of Fe–SBA-15 exhibits strong absorption bands only at 220–250 nm. These bands have been assigned to the ligand-to-metal charge transfer (LMCT) transition tetrahedrally oxygen-coordinated $[FeO_4]^-$ units and are characteristic of Fe in bulk silica. The main absorption feature of Fe–Ga–SBA-15 is at 270 nm. Moreover, the absorption band is significantly lower at a lower wavelength, implying that the Fe speciation differs strongly in these two materials.

We reported detailed findings of UV Raman spectroscopy of Fe–SBA-15 in previous works [14,23]. The bands at 490, 600, and 978 cm^{-1} are assigned to vibrations of the SBA-15 silica. The strong Raman bands at 510 and 1090 cm^{-1} are due to tetrahedrally coordinated Fe^{3+} ions (0.14 wt% Fe) in Fe–SBA-15 excited by a 244-nm laser. These bands are assigned to the symmetric and asymmetric Fe–O–Si stretching modes of Fe ions in the silica walls of Fe–SBA-15. The spectrum obtained with excitation at 325 nm does not show these two bands, because of the absence of resonance Raman enhancement. Indeed, the Raman bands related to Fe–O–Si stretching modes in materials with such a low Fe loading can be observed only when the excitation wavelength is close to the absorption wavelength [23]. Fig. 5 (below) shows the Raman spectra of Fe–Ga–SBA-15 excited by three different laser lines (244, 266, and 325 nm). The spectrum of Fe–Ga–SBA-15 excited by the 244-nm laser line exhibits bands at 1080 cm^{-1} and 1140 cm^{-1}, whereas in the spectrum obtained by excitation at 325 nm, only the band at 1140 cm^{-1} is present. The changes in the intensities of the bands at 1080 and 1140 cm^{-1} are due to the resonance effect resulting from changes in the excitation wavelength. Fe–Ga–SBA-15 contains mainly isolated Fe species in octahedral or pseudotetrahedral positions, as shown by the UV–Vis spectra. Because the band at 1140 cm^{-1} is absent in Fe–SBA-15, we

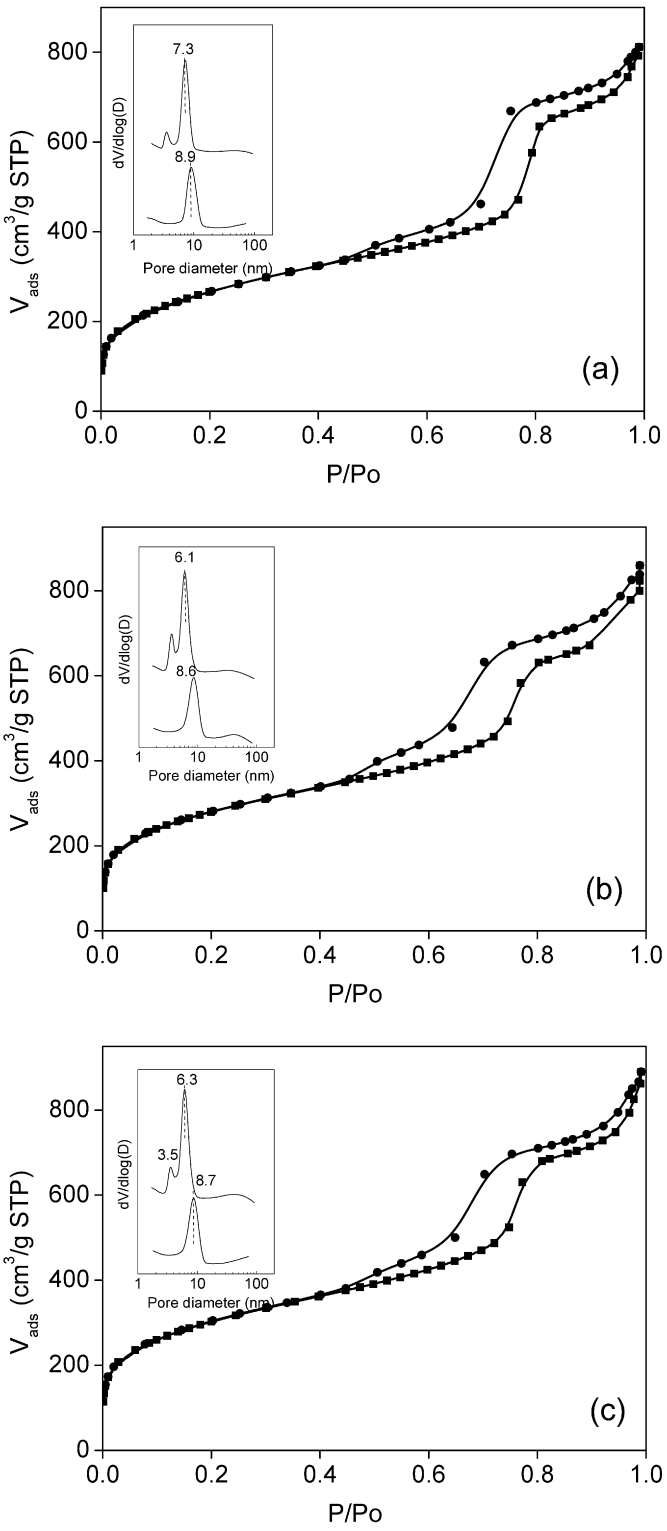

Fig. 2. Nitrogen adsorption–desorption isotherm and pore size distribution (inset) for (a) calcined Ga–SBA-15, (b) Fe–Ga–SBA-15(0.01) and (c) Fe–Ga–SBA-15(0.03).

assign this band to the isolated octahedral or pseudotetrahedral Fe^{3+} species at the surface of the SBA-15 silica. On normalizing the intensities of the bands at 1080 and 1140 cm^{-1} to the silica-specific band at 978 cm^{-1}, the ratio I_{1140}/I_{978} decreases from 1.9 for $\lambda_{exc} = 266$ nm to 1.6 for $\lambda_{exc} = 244$ nm

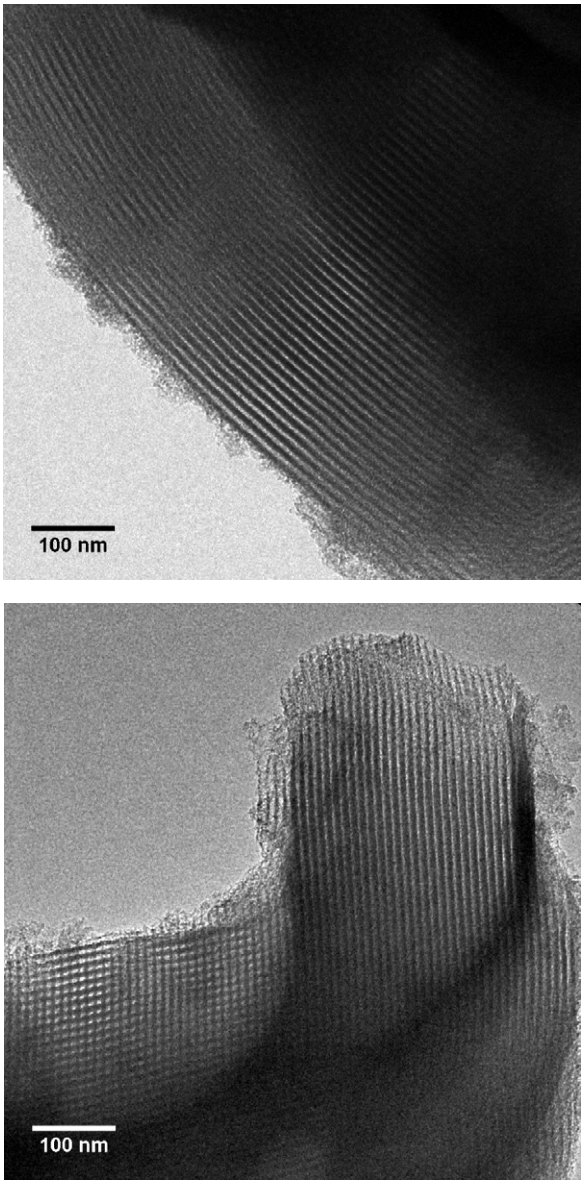

Fig. 3. Representative TEM images of calcined Fe–Ga–SBA-15(0.03).

and finally to 0.8 for $\lambda_{exc} = 325$ nm. These changes can be explained by the resonance Raman effect and are supported by the finding that the band's intensity is highest at $\lambda_{exc} = 266$ nm, which is closest to the absorption band of the dominant species in Fe–Ga–SBA-15 (270 nm). In agreement with earlier findings [23], the band at 1080 cm^{-1} could no longer be observed for $\lambda_{exc} = 325$ nm, because the excitation wavelength was too far from the absorption line of these tetrahedral Fe^{3+} species. This implies that the amount of tetrahedral Fe^{3+} in the silica phase is very low also for this sample, which agrees with the absence of strong absorption bands at lower wavelengths in the UV–Vis spectrum.

In summary, the combination of UV–Vis and resonance Raman spectroscopy has provided strong evidence that the simultaneous introduction of Ga and Fe in SBA-15 results in the preferential location of Fe^{3+} species at the surface of SBA-15. Because in the absence of Ga, the Fe^{3+} species end up predom-

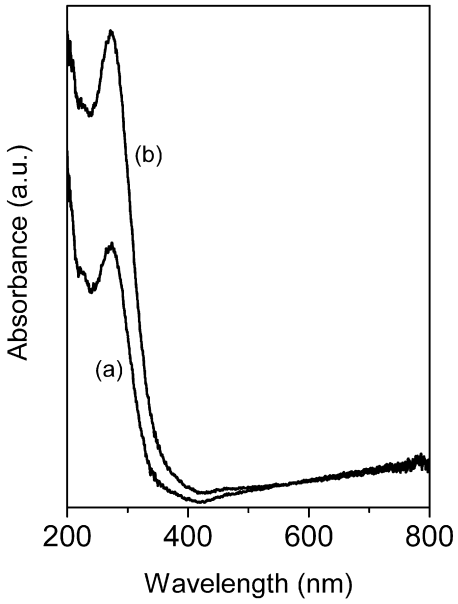

Fig. 4. UV–Vis absorption spectra of (a) Fe–Ga–SBA-15(0.01) and (b) Fe–Ga–SBA-15(0.03).

inantly in the silica phase, these Fe ions may compensate for the negative charge induced by substitutions of Si^{4+} by Ga^{3+} in the amorphous silica walls. This effect is very similar to the formation of surface Fe^{3+} species in Fe–Al–SBA-15 [14,15].

3.2. Catalytic performance

Fig. 6 presents the reaction rates of phenol as a function of the reaction time for Fe–Ga–SBA-15(0.01) and Fe–Ga–SBA-15(0.03) catalysts. Table 2 gives the corresponding reaction parameters. The conversion over Fe–SBA-15 is <0.1%, and the reaction rate of phenol is <0.01 mmol/g h. No formation of phenol is observed over Ga–SBA-15. This large difference in catalytic activity clearly demonstrates that Fe is necessary for benzene oxidation and that the presence of Ga leads to catalytically active Fe sites. From the characterization data, it follows that the presence of Ga results in the location of Fe^{3+} ions at the surface of the mesoporous silica; moreover, the isolated nature of the Fe^{3+} species is retained in the presence of Ga. The rate of phenol formation increases with iron content, consistent with the observation of increased formation of isolated Fe^{3+} ions by UV–Vis spectroscopy. In essence, these findings corroborate those reported earlier for Fe–Al–SBA-15 [15]. Fe–Al–SBA-15 exhibits activity in the oxidation of benzene to phenol, whereas Al–SBA-15 is inactive; thus, it may be concluded that the active sites in Fe–Ga–SBA-15 and Fe–Al–SBA-15 are very similar and consist of isolated Fe^{3+} sites. It is then straightforward to suggest that the Fe ions are stabilized at the surface, compensating for the negative charge induced by substitutions of Si^{4+} by Al^{3+} or Ga^{3+}. In previous work, we showed that such Fe^{3+} species are quite stable even in strong acidic solution [14].

Table 2 compares the benzene conversion and phenol selectivity for Fe–Ga–SBA-15(0.03) and Fe–Al–SBA-15 as a function of reaction time. Initially, the conversion of benzene for the Ga-based catalyst is >2% at a phenol selectivity of 45%. The

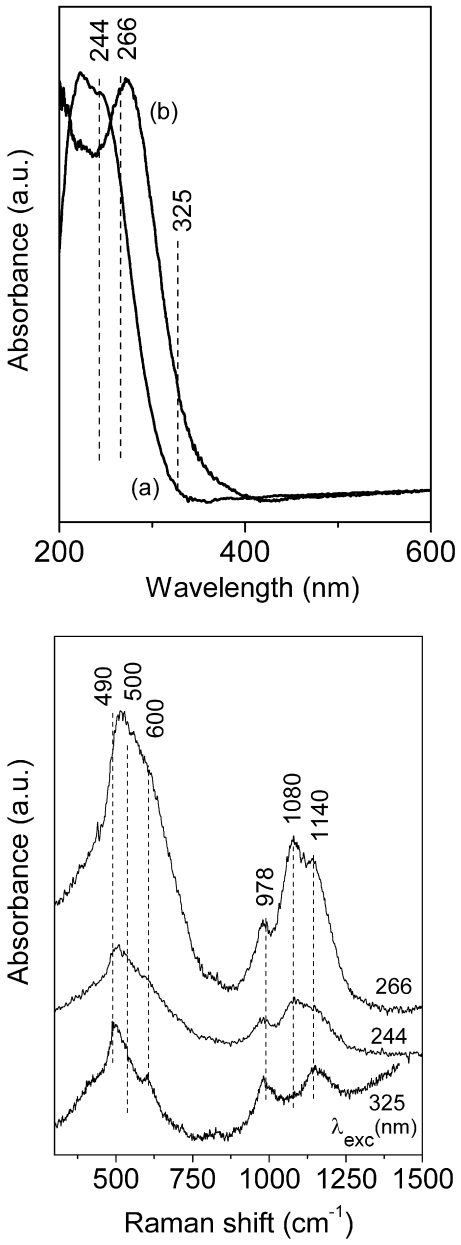

Fig. 5. (Above) Comparison UV–Vis absorption spectra of (a) Fe–SBA-15 and (b) Fe–Ga–SBA-15(0.03) and the position of laser lines used for Raman spectroscopy and (below) Raman spectra of Fe–Ga–SBA-15(0.03) with excitation at 244, 266 and 325 nm.

catalytic activity of Fe–Ga–SBA-15 is substantially lower than that of steam-activated FeZSM-5 catalysts [12]; moreover, the selectivity to the desired oxidation product is lower. In contrast, similar to what was observed for zeolites, phenol selectivity increases with decreasing conversion. After a reaction time of 1 h, the conversion becomes stable at around 1% with a phenol selectivity of 70%. Compared with the catalytic performance of Fe–Al–SBA-15 [15], the selectivity to phenol is higher for Fe–Ga–SBA-15 at the same Fe loading.

The number of active Fe^{2+} species was determined by titration with nitrous oxide at 523 K. The number of α-sites was evaluated by determining the amount of molecular nitrogen released during the decomposition of nitrous oxide at 523 K [13,

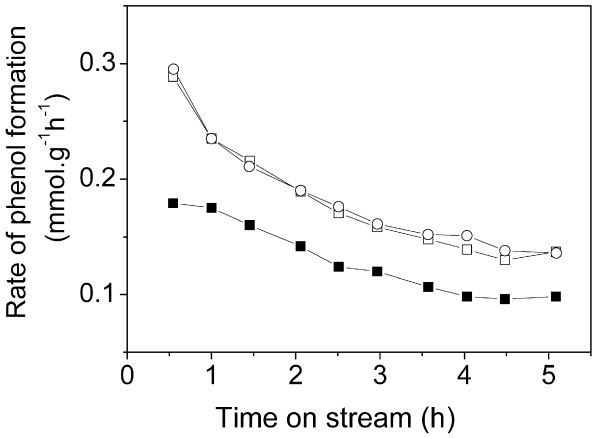

Fig. 6. Reaction rate of phenol as a function of reaction time for (■) calcined Fe–Ga–SBA-15(0.01), (□) Fe–Ga–SBA-15(0.03) and (○) Fe–Al–SBA-15 as a function of reaction time.

Table 2
Benzene conversion ($X_{C_6H_6}$), benzene selectivity to phenol ($S_{C_6H_6}$) for the various mesoporous catalysts during benzene oxidation

Catalyst	$t_R = 0.5$ h		$t_R = 1$ h		$t_R = 3$ h	
	$X_{C_6H_6}$	$S_{C_6H_6}$	$X_{C_6H_6}$	$S_{C_6H_6}$	$X_{C_6H_6}$	$S_{C_6H_6}$
Fe–Ga–SBA-15(0.03)	2.3	47	1.4	62	0.8	72
Fe–Al–SBA-15	5.0	27	3	30	2.5	26

24]. At this temperature, N_2O decomposes stoichiometrically to gaseous molecular nitrogen and surface oxygen species. The density of α-sites is 8.8×10^{-7} mol/g. As expected, such sites are absent in Fe–SBA-15 with similar Fe content, as well as in Ga–SBA-15 materials. The active site density of Fe–Ga–SBA-15 is similar to that of Fe–Al–SBA-15; thus, at similar Fe content in Fe–Al–SBA-15 and Fe–Ga–SBA-15, the α-site densities are nearly equal, as are the reaction rates for phenol. There is, however, a difference in conversion and selectivity, and tentatively this suggests that the intrinsic hydroxylation activity of the catalytically active sites is somewhat lower in Fe–Ga–SBA-15 than in Fe–Al–SBA-15. On the other hand, the selectivity is higher, which may indicate the lower tendency of Fe–Ga–SBA-15 to hydroxylate phenol to products that do not leave the catalyst surface. Thus, it appears that the catalytically active Fe sites have somewhat different chemical properties when bound to Ga or Al.

It also is important to note that the fraction of Fe ions in the SBA-15-based catalysts able to decompose nitrous oxide at low temperature is very low compared with the total Fe content (∼2.4%). As in the zeolite-based oxidation catalysts, here only a small fraction of Fe is in the active form. In the reference FeZSM-5 catalyst [12], about 15% of the Fe is in the active form. The remaining Fe species likely are inactive, because of their agglomeration during the steaming treatment to activate the zeolite precursor materials. Fe–Ga–SBA-15 is not steamed, and its physicochemical characterization points to a more uniform and isolated character of the Fe species in the active material. The relatively low fraction of catalytically active Fe species is likely related to the absence of short-range order in the mesoporous silicas. As reported earlier [15], the intrinsic activity of these mesoporous silicas is equal to that in zeolite-based systems. The catalytic activity of these mesoporous materials can be improved by bringing about crystallinity in their amorphous walls.

4. Conclusion

Highly ordered SBA-15 materials containing isolated Fe species stabilized by Ga^{3+} ions in the bulk of silica were successfully prepared by direct hydrothermal synthesis. The isolated nature of the Fe sites is characterized by an optical absorption band centered around 270 nm and a resonance Raman band at 1140 cm^{-1}. Some of the isolated Fe sites at the silica surface are active in the oxidation of benzene to phenol. Thus, SBA-15 silica can be functionalized by isolating Fe species at its surface. Such a material is catalytically active in the oxidation of benzene to phenol with nitrous oxide in a manner similar to that of FeZSM-5 zeolites.

Acknowledgments

This work was supported by the Programme for Strategic Scientific Alliances between China and the Netherlands, funded by the Royal Netherlands Academy of Arts and Science and the Chinese Ministry of Science and Technology (grant 04-PSA-M-01), the National Basic Research Program of China (grants 2003CB615806 and 2005CB221407), and the National Natural Science Foundation of China (grants 20773118 and 20673115).

References

[1] D. Zhao, J. Feng, Q. Huo, N. Melosh, G.H. Fredrickson, B.F. Chmelka, G.D. Stucky, Science 279 (1998) 548.
[2] S. Bordiga, R. Buzzoni, F. Geobaldo, C. Lamberti, E. Giamello, A. Zecchina, G. Leofanti, G. Petrini, G. Tozzola, G. Vlaic, J. Catal. 158 (1996) 486.
[3] A. Corma, M.S. Grand, A.V. Gonzalez, A.V. Orichilles, J. Catal. 159 (1996) 375.
[4] D. Zhao, Q. Huo, J. Feng, B.F. Chmelka, G.D. Stucky, J. Am. Chem. Soc. 120 (1998) 6024.
[5] W.H. Zhang, J. Lu, B. Han, M. Li, J. Xiu, P. Ying, C. Li, Chem. Mater. 14 (2002) 3413.
[6] A. Corma, M.S. Grand, A.V. Gonzalez, A.V. Orichilles, J. Catal. 159 (1996) 375.
[7] Y. Li, W.H. Zhang, L. Zhang, Z. Wei, Q. Yang, Z. Feng, C. Li, J. Phys. Chem. B 108 (2004) 9739.
[8] S. Wu, Y. Han, Y.C. Zou, J.W. Song, L. Zhao, Y. Di, S.Z. Liu, F.S. Xiao, Chem. Mater. 16 (2004) 486.
[9] J. Perez-Ramirez, F. Kapteijn, G. Mul, J.A. Moulijn, Chem. Commun. (2001) 693.
[10] G.I. Panov, CATTECH 4 (2000) 18.
[11] E.J.M. Hensen, Q. Zhu, R.A.J. Janssen, P.C.M.M. Magusin, P.J. Kooyman, R.A. van Santen, J. Catal. 233 (2005) 123.
[12] E.J.M. Hensen, Q. Zhu, R.A. van Santen, J. Catal. 233 (2005) 136.
[13] K. Sun, H. Zhang, H. Xia, Y. Lian, Y. Li, Z.C. Feng, P. Ying, C. Li, Chem. Commun. (2004) 2480.
[14] Y. Li, Z. Feng, H. Xin, F. Fan, J. Zhang, P.C.M.M. Magusin, E.J.M. Hensen, R.A. van Santen, Q. Yang, C. Li, J. Phys. Chem. B 110 (2006) 26114.
[15] Y. Li, H. Xia, F. Fan, Z. Feng, E.J.M. Hensen, R.A. van Santen, C. Li, Chem. Commun. (2008), in press.
[16] C. Li, J. Catal. 216 (2003) 203.

[17] S. Bordiga, A. Damin, F. Bonino, G. Ricchiardi, A. Zecchina, R. Tagliapietra, C. Lamberti, Phys. Chem. Chem. Phys. 5 (2003) 4390.
[18] G.A. Ricchiardi, S. Damin, S. Bordiga, C. Lamberti, G. Spano, F. Rivetti, A. Zecchina, J. Am. Chem. Soc. 123 (2001) 11409.
[19] C. Li, G. Xiong, Q. Xin, J.K. Liu, P.L. Ying, Z.C. Feng, J. Li, W.B. Yang, Y.Z. Yang, G.R. Wang, X.Y. Liu, M. Lin, X.Q. Wang, E.Z. Min, Angew. Chem. Int. Ed. 38 (1999) 2220.
[20] K.S.W. Sing, D.H. Everett, R.A.W. Haul, L. Moscou, R.A. Pierotti, J. Ronquerol, T. Siemieniewska, Pure Appl. Chem. 57 (1985) 603.
[21] S. Bordiga, R. Buzzoni, F. Geobaldo, C. Lamberti, E. Giamello, A. Zecchina, G. Leofanti, G. Petrini, G. Tozzola, G. Vlaic, J. Catal. 158 (1996) 486.
[22] C. Nozaki, C. Lugmair, A.T. Bell, T.D. Tilley, J. Am. Chem. Soc. 124 (2002) 13194.
[23] Y. Li, Z. Feng, Y. Lian, K. Sun, L. Zhang, G. Jia, Q. Yang, C. Li, Microporous Mesoporous Mater. 84 (2005) 41.
[24] K. Sun, H. Xia, E.J.M. Hensen, R.A. van Santen, C. Li, J. Catal. 238 (2006) 186.